Soft Matter

RSC Publishing

PAPER

View Article Online
View Journal | View Issue

Cluster formation in one-patch colloids: low coverage results

Cite this: *Soft Matter*, 2013, **9**, 2652

Gianmarco Munaò,* Zdenek Preisler, Teun Vissers, Frank Smallenburg and Francesco Sciortino

Received 29th October 2012
Accepted 11th December 2012

DOI: 10.1039/c2sm27490f

www.rsc.org/softmatter

We perform Monte Carlo simulations of a simple one-patch colloidal model to investigate the cluster formation and the phase behavior of the system on changing the width of the patch. We investigate the parameter region where the coverage (defined as the ratio between attractive and total surface) varies from 50% (the Janus case) to zero (hard-sphere). Simulation results indicate that on decreasing the coverage, particles self-assemble into clusters of different shapes, from micelles close to the Janus case, to one and two dimensional aggregates (wires and lamellae) for smaller coverage. Close to the hard-sphere limit, small micelles and dimers dominate the scene. We never find evidence of a gas–liquid (colloidal-rich/colloidal-poor) phase separation: it confirms that self-assembly into clusters which expose to their neighbors mostly repulsive surfaces suppresses phase separation and stabilizes cluster phases.

1 Introduction

Developments in particle synthesis are starting to provide a well-defined set of experimental methods for obtaining colloidal particles with different shapes, sizes and chemical compositions.[1–5] In this context, it has been possible to realize colloids with a pre-defined number of solvophilic and solvophobic regions on their surface, commonly named patchy particles.[6–9] Such colloidal particles, which exhibit strongly anisotropic interactions, have been recently investigated in detail experimentally[8,10–14] and using theoretical and simulation approaches.[7,9,15–33] While in the case of spherically symmetrical potentials a good understanding of phase diagrams, liquid structures and crystal phases in colloidal systems has been reached,[34,35] the structure and dynamics of patchy colloids is the subject of an intense current investigation.

An interesting class of patchy colloids is provided by particles with a single patch, having surface chemical properties differing from the remaining part of the particle. The so-called Janus colloids,[10,36–42] in which the patch covers one half of the particle surface, are among the most common examples. In spite of their apparent simplicity, Janus colloids have aroused increasing interest both for their potential technology application and in view of the peculiar self-assembly properties when compared to isotropic colloidal particles.[40,43]

Experimental results have shown that these particles self-assemble in several types of aggregates.[44,45] Granick and coworkers showed that charged Janus particles, with opposite electric charge on the two hemispheres, self-assemble into micelles, whose shape has been analyzed by combined epifluorescence microscopy and Monte Carlo simulation, with excellent agreement.[43] In a more recent study of Janus spheres with hemispherical hydrophobic attraction, the same group has documented the presence of fibrillar triple helices with up to six nearest neighbors per particle.[41] Finally, Janus particles have been employed for drug delivery systems to deliver multiple payloads with different solubilities.[46]

In this article, we investigate a simple model of patchy particle with one attractive patch, for values of the coverage χ smaller than the Janus case ($\chi = 0.5$). χ is defined as the ratio between the surface of the attractive patch and the total sphere surface. To this aim we select the one-patch Kern and Frenkel (KF)[15,47] model, in which the colloidal particle is described as a hard sphere decorated with one circular patch located on the surface. This model can be considered an extension to the colloid world of the so-called primitive models of associating particles, introduced in the 80's[48–52] in the context of molecular fluids. In the KF model, two particles interact if their mutual distance is within the range of the attraction, modeled by a square-well (SW) contribution and if their patches are properly aligned with each other. This model allows us to interpolate continuously from the SW isotropic potential (when the entire surface of the sphere is attractive) to the Janus case (when only one hemisphere is attractive), to the hard-sphere case (when the patch width vanishes). The dependence of the thermodynamic properties of the one-patch KF model, on going from the SW to the Janus case, has been recently investigated.[29] It has been shown that on decreasing the patch width, the SW critical point shifts to lower temperatures T^* and lower densities ρ, an effect driven by the progressive decrease of the

Dipartimento di Fisica, Sapienza, Università di Roma, Piazzale A. Moro 5, 00185 Roma, Italy. E-mail: gmunao@gmail.com

attractive component. Interestingly, when the Janus limit is approached, colloids reproduce the behavior of amphiphilic molecules in which the hydrophilic hemisphere is mimicked by the repulsive hard sphere potential and the hydrophobic part by the attractive SW contribution. Indeed, it has been demonstrated[53] that the combined features of the equal amplitude of the hemispheres along with the specificity of the interaction potential give rise to a micellization process that deeply influences the phase diagram of the system: the self-aggregation destabilizes the usual condensation process, providing a re-entrant binodal curve shifted towards higher densities as the system is cooled. The micellization process competes with the phase separation *via* the thermodynamic stabilization of essentially non-interacting aggregates,[53] providing a clear example of the interplay between self-assembly and macroscopic phase separation.[54] A recent application of the Barker–Henderson (BH) thermodynamic perturbation theory to the KF model[20] has shown that when $\chi > 0.5$, theoretical predictions for the phase diagram closely follow simulation results. However, theoretical predictions break down when the Janus limit is reached and are not able to describe the anomalous thermodynamic behavior.[53] Approaches based on integral equation theories[27,55] also fail when χ decreases significantly with respect to the SW case, leaving the simulations as a main tool for describing the low coverage behavior of this class of one-patch colloids.

In this article we report a Monte Carlo (MC) simulation study of the Kern–Frenkel model from the Janus case down to the hard-sphere case, providing a complete picture of the behavior of this model for all possible patch widths. We focus our investigation on the self-assembly process, analyzing in detail the size and the shape of aggregates, paying attention to the influence of the aggregation process on the phase behavior and on the structure of the system.

This paper is organized as follows: in Section II we describe the KF model and provide details on the simulations. Results are presented and discussed in Section III, analyzing separately the different patch widths investigated. Conclusions follow in Section IV.

2 Model and simulation approaches

The model chosen was developed by Kern and Frenkel[15] in the context of colloidal systems with strongly directional attractions. It constitutes a simple model for patchy colloids, largely adopted to investigate structure, thermodynamics and self-assembly in such systems.[27–29,53,56] In this scheme two particles are bonded if their mutual distance is less than a predefined range and the vector joining the centers of mass intersects the attractive patches on the surfaces of both spheres. The model is schematically depicted in Fig. 1. Following KF, the pair potential is written as a product of a SW potential with an angular contribution:

$$\Phi(12) = \phi(r_{12})\cdot\psi(\hat{\boldsymbol{n}}_1,\hat{\boldsymbol{n}}_2,\hat{\boldsymbol{r}}_{12}) \quad (1)$$

where

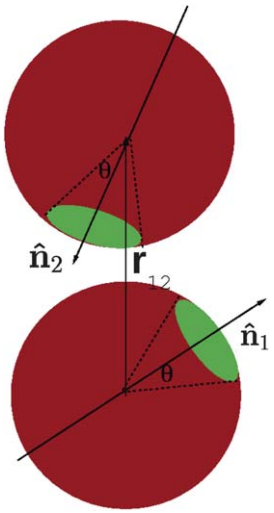

Fig. 1 Model of patchy particles investigated in this work. The surface of each sphere is divided into an attractive part (green) and a repulsive part (red). Unit vectors $\hat{\boldsymbol{n}}_1$ and $\hat{\boldsymbol{n}}_2$ indicate the patch position, whereas the vector $\boldsymbol{r}_{12}$ joins the centers of the two particles.

$$\phi(r) = \begin{cases} \infty & \text{if} \quad 0 < r < \sigma \\ -\varepsilon & \text{if} \quad \sigma < r < \sigma + \lambda\sigma \\ 0 & \text{if} \quad r > \sigma + \lambda\sigma \end{cases} \quad (2)$$

and

$$\psi\left(\hat{\boldsymbol{n}}_1, \hat{\boldsymbol{n}}_2, \hat{r}_{12}\right) = \begin{cases} 1 & \text{if} \quad \hat{\boldsymbol{n}}_1\cdot\hat{\boldsymbol{r}}_{12} \geq \cos\theta \\ & \text{and} \quad \hat{\boldsymbol{n}}_2\cdot\hat{\boldsymbol{r}}_{12} \leq -\cos\theta \\ 0 & \text{otherwise} \end{cases} \quad (3)$$

In eqn (1)–(3), θ is the angular semiamplitude of the patch, σ is the hard core diameter, $\lambda\sigma$ is the range of the square-well potential and ε is the depth of the well. In all calculations we assume $\lambda = 0.5$. This value has been used in the previous study of the same model for $0.5 < \chi < 1$ (ref. 20, 29 and 53) and it is here retained to provide a complete characterization for this range. The quantities $\hat{\boldsymbol{n}}_1$ and $\hat{\boldsymbol{n}}_2$ are unit vectors that provide the patch position in particles 1 and 2, respectively. The unit vector $\hat{\boldsymbol{r}}_{12}$ is directed along the line connecting the centers of mass of the two spheres. The advantage of this model lies in the possibility to tune in a continuous way the percentage of the attractive surface on the sphere by simply varying the value of θ, from a fully isotropic square-well ($\theta = \pi$) to the purely hard sphere case ($\theta = 0$). The ratio between the size of the patch and the whole surface of the sphere is defined as the particle coverage χ related to the angular semiamplitude by:

$$\chi = \sin^2(\theta/2) = \frac{1-\cos(\theta)}{2} \quad (4)$$

In the following, σ provides the unit of length and ε the unit of energy. The reduced temperature T^* is expressed in units of ε, (*i.e.* Boltzmann constant $k_B = 1$).

Standard Monte Carlo (MC) simulations at constant volume and temperature (NVT ensembles) have been carried out on a

sample constituted by $N = 2000$ particles enclosed in a cubic box with standard periodic boundary conditions. In all simulations, translational and rotational moves consisting of a maximum random translation of $\pm 0.1\sigma$ and a maximum random rotation of ± 0.1 rad of a randomly selected particle have been implemented.

This choice of N guarantees that, even when large aggregates have formed, a sufficiently large number of clusters is simultaneously present in the simulation box. Long simulation runs (of the order of 10^8 to 10^9 MC steps) have been performed to reach equilibrium. We found that in some cases, the system did not fully equilibrate even after months of simulation time, due to a very slow aggregation process. These cases are indicated in the text. A MC step is here defined as N attempts to rotate and translate a particle.

3 Results and discussion

In order to clarify the structures of the aggregates and some thermodynamic properties of the model, we discuss separately the four investigated values of χ. We recall the reader that the case $\chi = 0.5$ (the Janus case) has been already extensively investigated in ref. 29 and 53. There, it has been shown that the gas–liquid phase separation (observed also for larger coverage), interferes with the self-assembly of particles into micelles and vesicles, providing a clear example of the effect of the competition within these two phenomena.

In the following, we discuss the aggregates observed in simulations for different values of T^*, ρ and χ. To define the nomenclature we provide in Fig. 2 a sketch of the different cluster shapes which will be further described in the following: oligomers (O), micelles (M), wires (W) and lamellae (L). These aggregates originate cluster phases (characterized by a dominant peak in the cluster size distribution at finite size value) or macroscopic phases (L).

We note that in this study we focus on structures that spontaneously form but we are aware that there is a need for understanding the differences between kinetically stabilized and thermodynamically stabilized structures. It is also worth mentioning that free-energy calculations require the evaluation of the equation of state for the partially ordered phases (wires and lamellar phases) which are quite computationally demanding already at the temperatures investigated here. We plan to address the issue of the thermodynamic stability in a future work. As a guide to characterize the clusters, we also note that the coverage controls the maximum number of bonds which can be formed. Since the potential is not short-ranged, this number does depend on the potential range. For the present model, the observed maximum number of bonds N_{max} that a single particle can form for the different χ values investigated, expressed as (χ, N_{max}) is: (0.4,11), (0.3,10), (0.2,6), (0.1,4). However, it does not necessarily imply that extended structures can be formed in which all particles satisfy the maximum possible number of contacts. Since the (average) number of bonds per particle is limited by the geometrical constraints of the structure that they are in, the average number of bonds per particle will in practice often be lower even at low temperature.

3.1 $\chi = 0.4$

We start our investigation by discussing the case in which forty percent of the particle surface is attractive ($\chi = 0.4$, corresponding to $\cos\theta = 0.2$). The behavior of the average potential energy per particle $\langle E_i \rangle$, defined as the total potential energy divided by the number of particles, along various isotherms is shown in Fig. 3. At all $T^* > 0.21$, the ρ dependence of $\langle E_i \rangle$ is not very significant. At $T^* = 0.20$, a jump in $\langle E_i \rangle$ is observed on increasing ρ. The ρ-independence of the energy is typical of self-assembly processes, where a density increase is associated with a progressive concentration of almost non-interacting aggregates of the same shape and size.

In previous studies of Janus colloids[53] it has been shown that at low T^* the system self-assembles into well-defined spherical clusters which maintain their properties in a wide region of ρ. The most frequent clusters observed for the KF-Janus colloids are micelles, in which about 10 particles are bounded, and vesicles, multilayer aggregates of about 45 particles.

The reduction of the coverage from 0.5 to 0.4 is sufficient to destabilize the formation of vesicles, which are rarely observed. Instead micelles are still present in large amounts, especially at the lowest ρ. To visualize the structure of the system for $\chi = 0.4$, we show in Fig. 4 snapshots of typical configurations for two different T^* and various ρ. At $T^* = 0.25$ (top row in Fig. 3), the

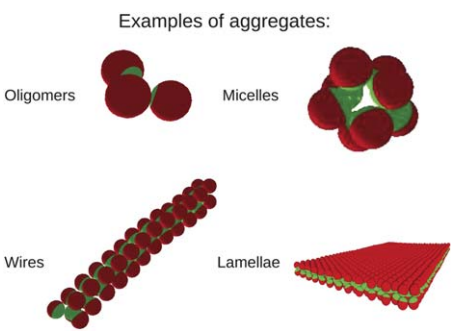

Fig. 2 Sketch of different aggregates observed in this work.

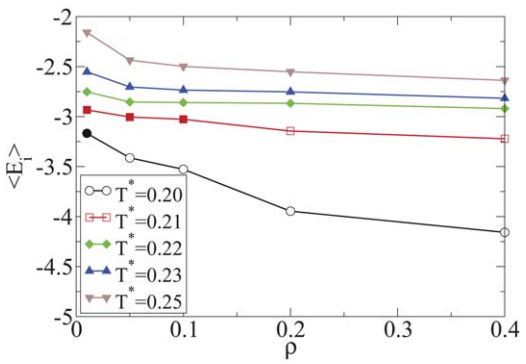

Fig. 3 Average potential energy per particle $\langle E_i \rangle$ *vs.* number density ρ for $\chi = 0.4$ along various isotherms. Open symbols refer to not fully equilibrated configurations.

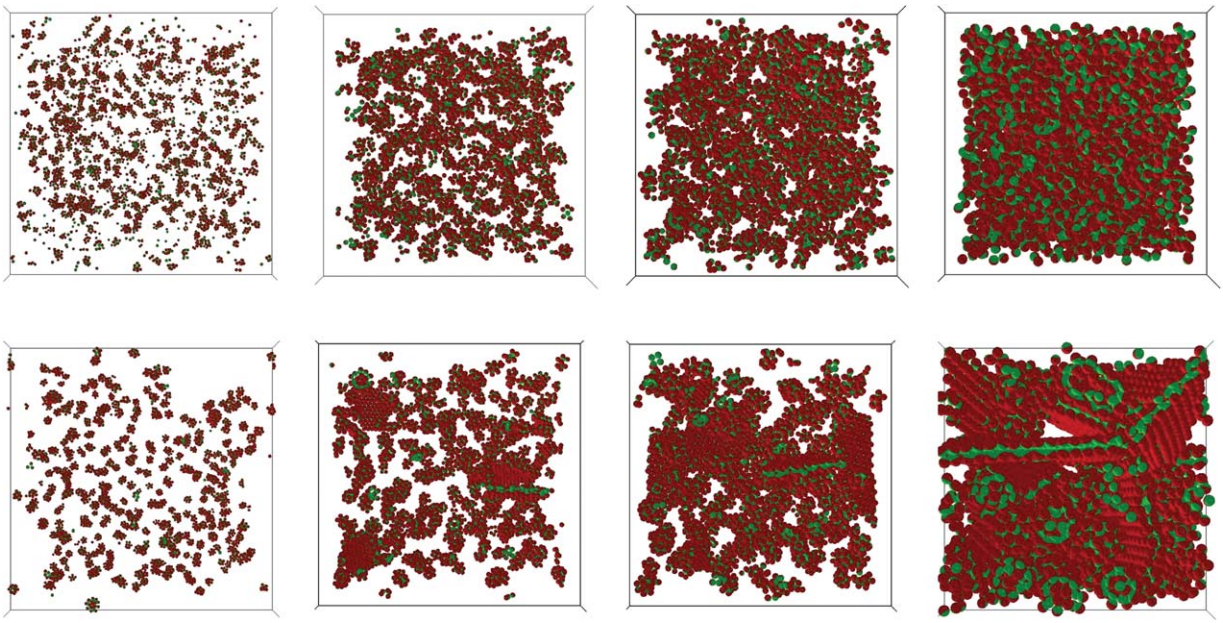

Fig. 4 Snapshots of particle configurations at fixed $\chi = 0.4$, $T^* = 0.25$ (top) and $T^* = 0.20$ (bottom) and $\rho = 0.01$, $\rho = 0.05$, $\rho = 0.1$ and $\rho = 0.4$. Density increases from left to right.

system is composed at all densities by micelles exposing the repulsive part and encapsulating the attractive one. Each particle in the micelle is able to form about six bonds with their neighbors (corresponding to an average energy per particle of about −3.0). The snapshots shown in the bottom panels ($T^* = 0.20$) give a rather different picture. On increasing the density, the micellar phase transforms into a lamellar one, in which each particle is bonded with approximately nine neighbors. Although the simulations at low T^* do not allow for a proper equilibration, nuclei of the lamellar phase suggest the presence of a coexistence region between micelles and lamellae which extends to low ρ. The analysis of the distributions of the energy per particle E_i confirms the structural change highlighted by the snapshots. E_i is calculated as the sum of the pair interaction energies of all j neighbors of a given i particle, *i.e.* $E_i \equiv \Sigma_j E_{ij}$. Fig. 5 shows indeed that for $\rho \geq 0.05$, the micellar peak at $E_i = -6$ crosses toward the lamellar peak at $E_i = -9$. Differently from the Janus case[53] ($\chi = 0.5$), we do not observe hints of gas–liquid phase separation at this value of χ. The absence of phase separation can have two origins: (i) on the one hand it can be the result of a further stabilization of the cluster phase of micelles which would destabilize critical fluctuations, thus eliminating the critical point; as a consequence, particles are not able to form a percolating network of bonds, a pre-requisite for phase separation. On the other hand (ii), it can be pre-empted by the formation of a lamellar phase, eliminating the possibility of observing the (metastable) critical point. We have checked with grand canonical MC simulations that, down to $T^* = 0.215$, density fluctuations are described by a unimodal distribution, characteristic for homogeneous systems. We also note that the theory developed in ref. 20, which has been very successful in predicting the location of the critical point for $\chi > 0.5$, predicts a critical point for $\chi = 0.4$ at $T_c \approx 0.2$ and $\rho_c \approx 0.1$,

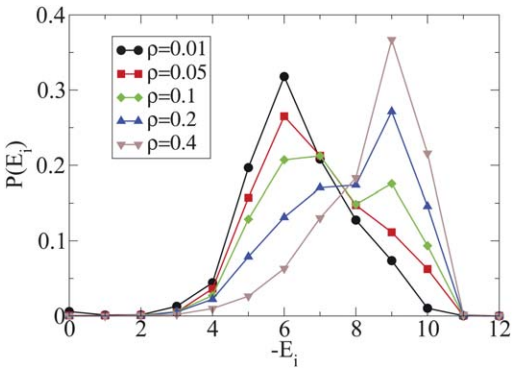

Fig. 5 Histogram of the total energy per particle E_i at fixed $\chi = 0.4$ and $T^* = 0.20$ for different ρ.

well inside the region where lamellae are stable. Thus, although we cannot exclude *a priori* case (i), we suspect that for $\chi = 0.4$, self-assembly into lamellae has suppressed the possibility of a critical point.

Finally, we show in Fig. 6 the qualitative phase diagram for $\chi = 0.4$, in which the micelles and lamellar phases are indicated.

3.2 $\chi = 0.3$

Next we investigate the case $\chi = 0.3$. Interestingly, Fig. 7 shows the presence of a drop in the ρ dependence of $\langle E_i \rangle$ at large ρ, already when $T^* = 0.145$, suggesting the presence of a new phase competing with micelles. The snapshots of the configurations (Fig. 8) show that the system forms very long wires. Wires for $\chi = 0.3$ play the same role as lamellae for $\chi = 0.4$, both providing an ordered structure which becomes stable at low T^*.

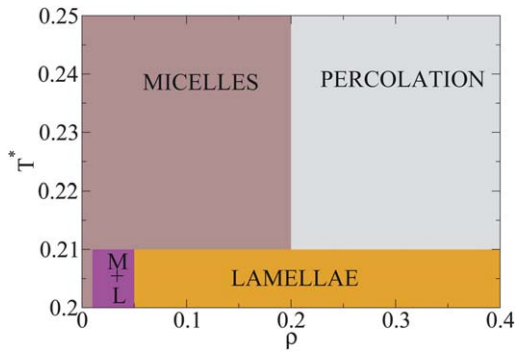

Fig. 6 Qualitative phase diagram of the Kern–Frenkel model at $\chi = 0.4$.

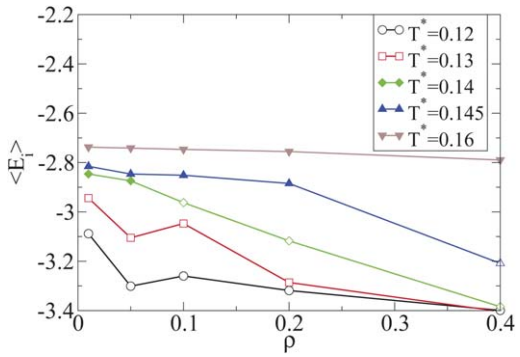

Fig. 7 Average potential energy per particle $\langle E_i \rangle$ *vs.* number density ρ for $\chi = 0.3$ along various isotherms. Open symbols refer to not fully equilibrated configurations.

Formation of long wires is often found in the self-assembly of biological systems.[57–59] The transition from spherical micelles to very long wires has recently been observed also in experimental studies of peptide amphiphiles[2] and nonionic surfactants:[60] it has been demonstrated that the increase of the hydrophobicity of the peptides as well as the asymmetric form of surfactants may transform the self-assembled nanostructures from spherical micelles and vesicles to wires, ribbons and cylinders.

These experimental results indicate that the micelle–wire transition appears under some well defined conditions: one of these is the anisotropy of the interaction, which plays an important role for surfactants and peptide amphiphiles. From a theoretical point of view, free-energy calculations for long wires are not straightforward because of significant finite-size effects. As a consequence, the thermodynamic stability of the wire phase is still an open point, currently under examination. Fig. 9 graphically displays the T^*-dependence of the structural evolution at fixed $\rho = 0.05$. Even at this low ρ the micelle–wire transition is clearly visible. The aggregation process that generates the wires requires very long simulation times (more than 10^8 and, at the lowest investigated T^*, one order of magnitude more). Simulations at $T^* < 0.14$ do not equilibrate even in such a long time. The number of bonds in the system steadily increases with time, while wires become longer and longer. This is consistent with the experimental results by Kegel and coworkers,[3] which describe the disordered wires phase as a non-equilibrium cluster state.

The sudden appearance and continued growth of the wires suggests that a free energy barrier exists between micelle-like and wire-like clusters, resulting in a nucleation and growth scenario. In this case, hysteresis could prevent wires from

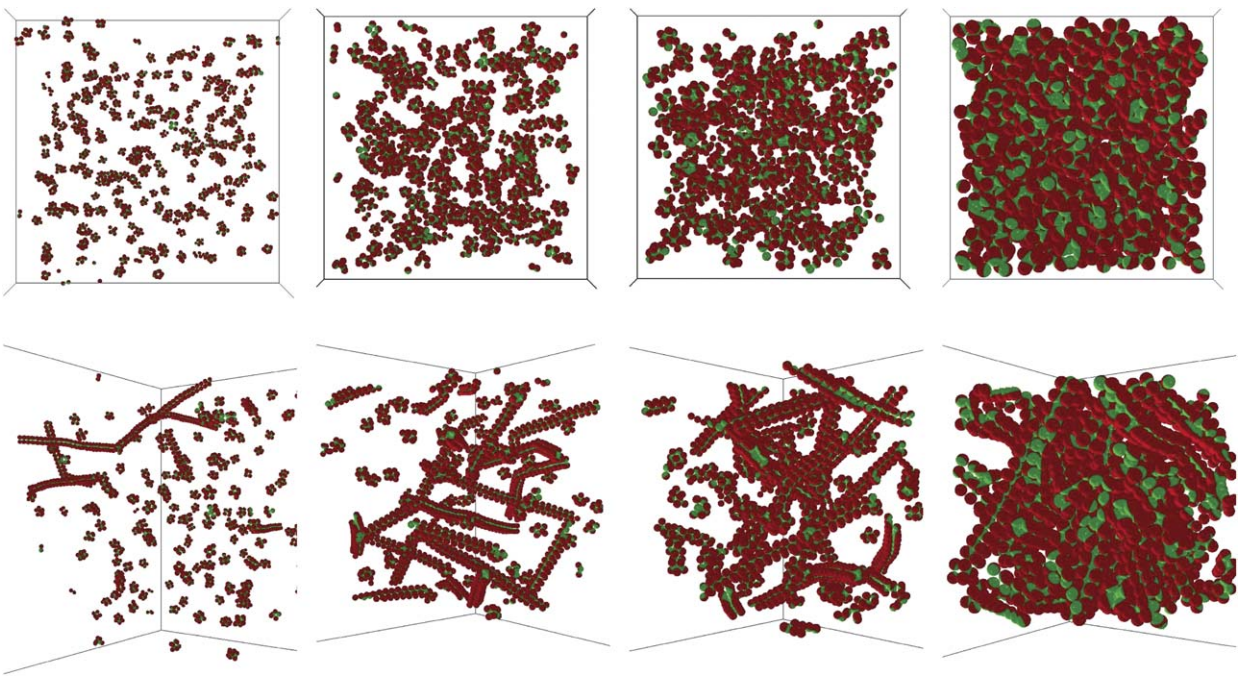

Fig. 8 Snapshots of particle configurations at fixed coverage $\chi = 0.3$ and temperatures $T^* = 0.16$ (top) and $T^* = 0.12$ (bottom). Density values are the same as in Fig. 4.

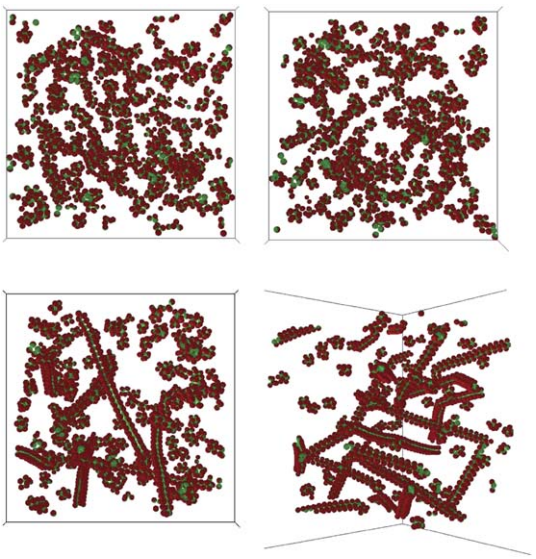

Fig. 9 Snapshots of particle configurations at fixed $\chi = 0.3$, $\rho = 0.05$ and $T^* = 0.15$, $T^* = 0.14$, $T^* = 0.13$ and $T^* = 0.12$. T^* decreases from left to right and from top to bottom.

forming spontaneously until the combination of temperature and density is such that only extremely long wires are stable, which are almost impossible to equilibrate in simulations and are likely affected by strong finite-size effects. It is even possible

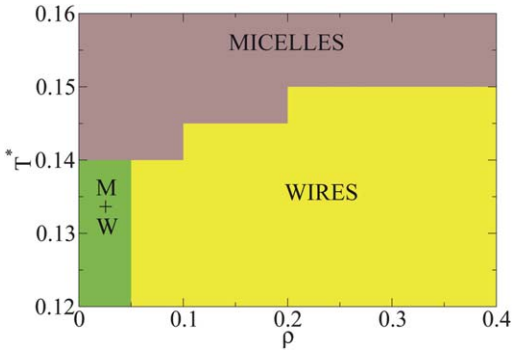

Fig. 11 Qualitative phase diagram of the Kern–Frenkel model for $\chi = 0.3$.

that sufficiently long wires (in the presence of smaller clusters) would spontaneously order. For example, the disordered wire phase shown in the bottom panel of Fig. 8 may well be only kinetically trapped on the way to forming a stable ordered crystal. We report in Fig. 10 the histograms of the total energy per particle E_i (a) at fixed $\rho = 0.05$ for four values of T^* along with the corresponding cluster size distributions (b). At $T^* > 0.13$ the plot of energies shows a maximum at $E_i = -5$, corresponding to a picture in which spherical micelles are the most diffused clusters. Upon lowering T^*, the maximum shifts towards $E_i = -7$. This behavior confirms the onset of a geometrical arrangement where one particle is coordinated with about five neighbors in the micellar structure, but is bonded with seven other particles, in the wires geometry. The

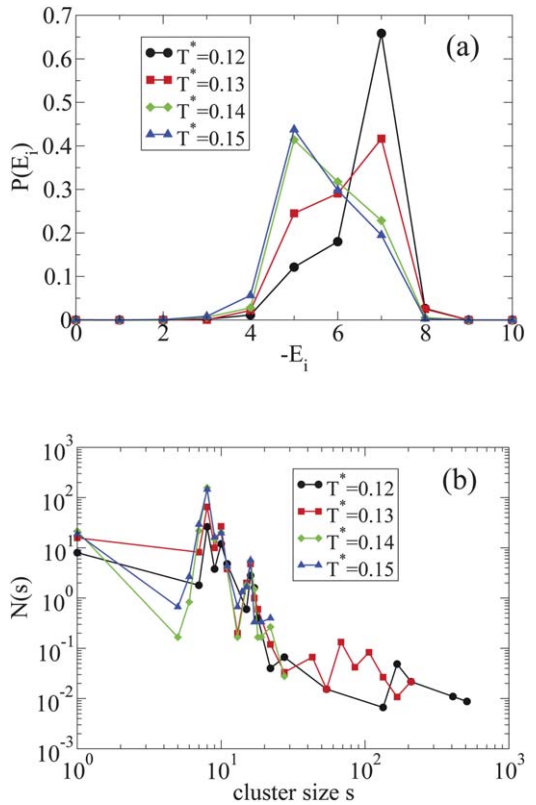

Fig. 10 (a) Histogram of the total energy per particle E_i at fixed $\chi = 0.3$ and $\rho = 0.05$ for different temperatures. (b) Cluster size distribution $N(s)$ at the same state points. Note that the normalization of $N(s)$ is such that $\sum_s sN(s) = N$.

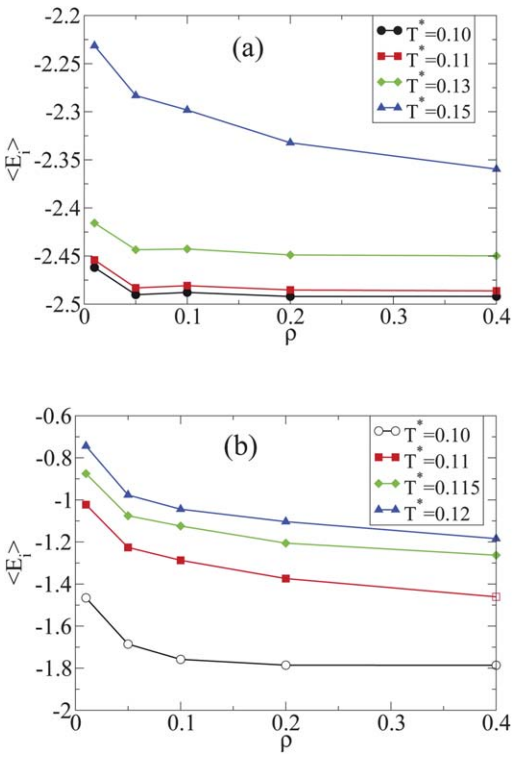

Fig. 12 Average potential energy per particle $\langle E_i \rangle$ *vs.* number density ρ for $\chi = 0.2$ (a) and $\chi = 0.1$ (b) along various isotherms. Open symbols refer to not fully equilibrated configurations.

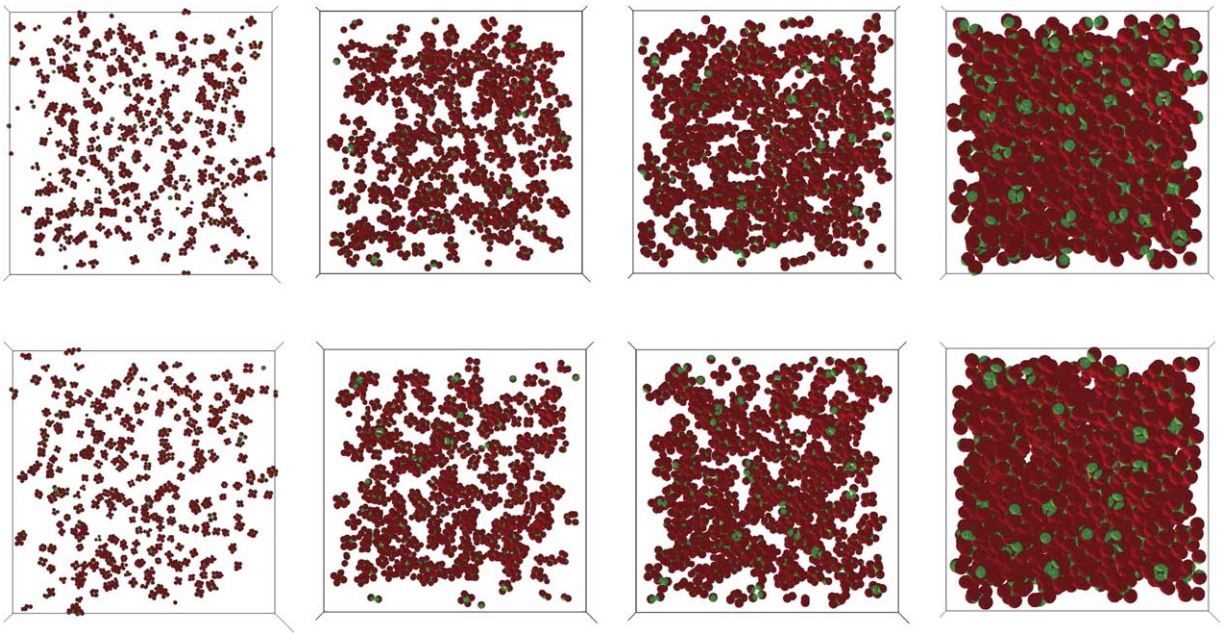

Fig. 13 Snapshots of particle configurations at fixed coverage $\chi = 0.2$ and temperatures $T^* = 0.15$ (top) and $T^* = 0.10$ (bottom). Density values are the same as in Fig. 4.

cluster size distribution $N(s)$, reported in panel (b) of Fig. 10, further clarifies the physical scenario: at high T^*, the majority of clusters have a small size, and $N(s)$ shows a well defined peak centered at cluster size $s = 8$. At low T^* only few small clusters are left and an increasing number of big wire-shaped clusters is observed. The qualitative phase diagram for $\chi = 0.3$ is reported in Fig. 11.

3.3 $\chi = 0.2$ and $\chi = 0.1$

We conclude the investigation by discussing the cases of $\chi = 0.2$ and $\chi = 0.1$, which behave similarly in their physical behavior. Differently from $\chi = 0.4$ and $\chi = 0.3$, both the wire structures as well as the lamellar phase are not observed and only micelles are found. The attractive patches are so small that it becomes impossible to create extended low-energy structures. Fig. 12

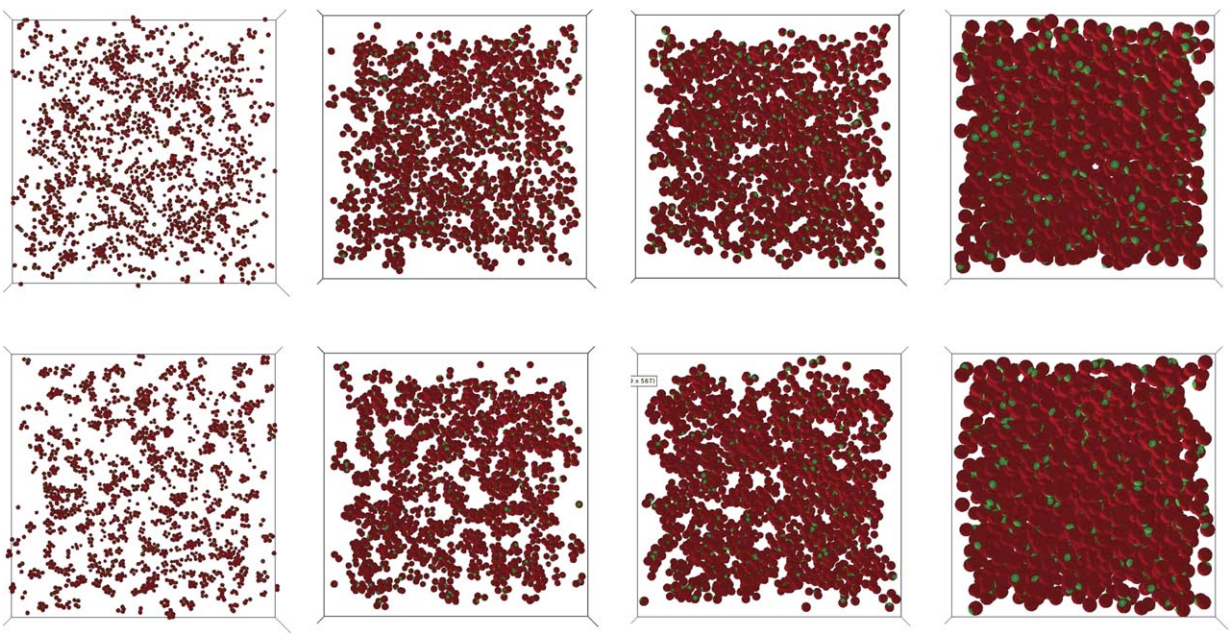

Fig. 14 Snapshots of particle configurations at fixed coverage $\chi = 0.1$ and temperatures $T^* = 0.12$ (top) and $T^* = 0.10$ (bottom). Density values are the same as in Fig. 4.

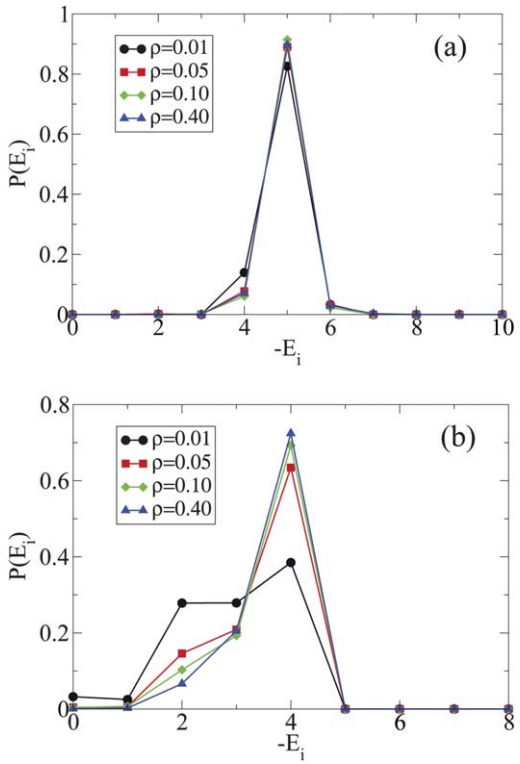

Fig. 15 Histograms of the total energy per particle E_i at fixed $T^* = 0.10$ and various ρ: (a), $\chi = 0.2$; (b), $\chi = 0.1$.

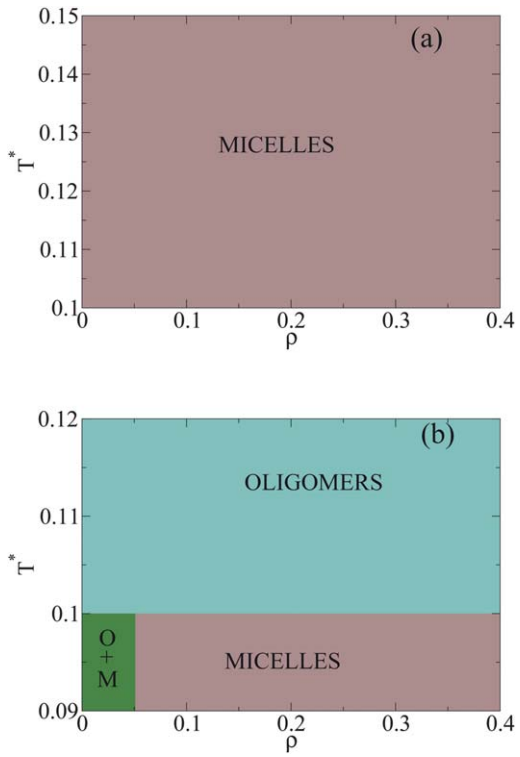

Fig. 16 Qualitative phase diagram of the Kern–Frenkel model for $\chi = 0.2$ (a) and $\chi = 0.1$ (b).

shows the average potential energy for $\chi = 0.2$ (a) and $\chi = 0.1$ (b): the absence of any anomalous trend suggests that the micelles formation is the only aggregation process observed under these conditions. The cluster size distributions, not reported here, show that only small spherical aggregates, mostly of size 6, are present. A percolating structure of bonded particles is never achieved. Each particle in the micelle tends to form 5 bonds when $\chi = 0.2$, and 4 bonds when $\chi = 0.1$. Consistent with the absence of a percolation of bonds, we do not observe any evidence of a gas–liquid phase separation. Fig. 13 shows the snapshots of equilibrated configurations for $\chi = 0.2$: no significant changes with T^* are evident, since particles have already reached their lowest energy state. At $\chi = 0.1$, the formation of micelles is preceded by the formation of small oligomers, as shown in the bottom panel of Fig. 14. These little structures are constituted by a small number of particles ($\simeq 3$) and do not show the spherical arrangement typical of the micelles. Furthermore, they appear to be the most favored configuration at low density, since the small value of the coverage along with the relatively high distance between the particles tends to promote the development of such small aggregates. With the aim to further analyze the bond distribution, we plot in Fig. 15 the distribution of the energy per particle, calculated at the lowest T^* investigated, namely $T^* = 0.10$, for both χ values.

We notice that for $\chi = 0.2$, the distribution does not show any remarkable difference upon varying ρ and there is only a sharp, well defined, peak at $E_i = -5$, confirming that micelles are the most stable clusters for all densities. Conversely, the energy distribution for $\chi = 0.1$ is a double-peaked function when ρ is low enough, namely $\rho = 0.01$, and develops a sharp peak at $E_i = -4$ when ρ increases. The first peak observed for $\rho = 0.01$ is placed at $E_i = -2$ and testifies the presence of small oligomers, eventually evolving in micelles for higher values of ρ. We note on passing that theoretical predictions from BH thermodynamic perturbation theory predict the critical points at $(T^* = 0.080, \rho = 0.075)$ for $\chi = 0.2$ and $(T^* = 0.036, \rho = 0.065)$ for $\chi = 0.1$, well inside the micellar region. To summarize these results, we show in Fig. 16 the phase diagrams for both cases; apart from the formation of the small oligomers observed for $\chi = 0.1$, no difference between them is found.

4 Conclusions

We have performed a simulation study of the Kern–Frenkel model for one-patch colloids, investigating the phase behavior and the self-assembled clusters when the coverage of the system is reduced below the Janus limit.

For none of the investigated χ values has a gas–liquid critical point been located, suggesting that for the investigated range the Janus case is indeed the limiting value for observing critical fluctuations in this class of models. We have observed that, for $\chi = 0.3$ and $\chi = 0.4$, extended low-energy structures form, which become stable upon cooling. For the case of $\chi = 0.4$ the observed structure is a lamellar phase, while for $\chi = 0.3$ it is a phase containing long wires. The enhanced stability of these structures is one possible reason for explaining the absence of

phase separation between disordered phases. According to this scenario, the gas–liquid critical point would be located well inside the stability region of the lamellar or wires phase, so deep that nucleation of the stable phase pre-empts the possibility to observe the metastable gas–liquid critical point. A further possibility for explaining the absence of criticality arises from the competition between the self-assembly process into mostly non-interacting micelles and the development of thermal correlations. The possibility of forming local dense regions (the micelles) which expose to the external world only their repulsive surface provides an efficient mechanism to prevent the formation of an extended network of bonds, and hence any critical phenomenon.

Finally, for $\chi = 0.2$ and $\chi = 0.1$ we do not observe any development of large aggregates in the system and the only observed clusters are constituted by small oligomers eventually evolving in spherical micelles when T^* is low enough. In this case, no extended low energy structures can form, proving that for these coverage values, it is indeed the self-assembly into micelles which do not attract each other (since all particles of the micelle expose the repulsive part of their surface) that prevents the gas–liquid separation.

The large variety of aggregates observed, from little oligomers and micelles to long wires and large lamellae, is dependent on both χ and T^* and constitutes one of the most interesting physical features of such colloids. The question regarding the influence of the range width is still open and it will constitute the subject of a further investigation. Such a study would complement the present one and provide further information on the best way to control and understand the sensitivity of cluster aggregates to the inter-particle interaction.

Acknowledgements

We acknowledge support from ERC-226207-PATCHYCOLLOIDS and ITN-234810-COMPLOIDS.

References

1 A. P. R. Eberle, R. Castañeda-Priego, J. M. Kim and N. J. Wagner, *Langmuir*, 2012, **28**, 1866.
2 Q. Meng, Y. Kou, X. Ma, Y. Liang, L. Guo, C. Ni and K. Liu, *Langmuir*, 2012, **28**, 5017.
3 T. H. Zhang, J. Klok, R. H. Tromp, J. Groenewold and W. K. Kegel, *Soft Matter*, 2012, **8**, 667.
4 S. Sacanna and D. J. Pine, *Curr. Opin. Colloid Interface Sci.*, 2011, **16**, 96.
5 Y. Wang, Y. Wang, D. R. Breed, V. N. Manoharan, L. Feng, A. D. Hollingsworth, M. Weck and D. J. Pine, *Nature*, 2012, **491**, 51.
6 V. N. Manoharan, M. T. Elsesser and D. J. Pine, *Science*, 2003, **301**, 483–487.
7 S. C. Glotzer and M. J. Solomon, *Nat. Mater.*, 2007, **6**, 557–562.
8 A. B. Pawar and I. Kretzschmar, *Macromol. Rapid Commun.*, 2010, **31**, 150–168.
9 Z. Zhang and S. C. Glotzer, *Nano Lett.*, 2004, **4**, 1407.
10 L. Hong, A. Cacciuto, E. Luijten and S. Granick, *Langmuir*, 2008, **24**, 621–625.
11 D. J. Kraft, J. Groenewold and W. K. Kegel, *Soft Matter*, 2009, **5**, 3823–3826.
12 Q. Chen, S. C. Bae and S. Granick, *Nature*, 2011, **469**, 381.
13 D. J. Kraft, J. Hilhorst, M. A. P. Heinen, M. J. Hoogenraad, B. Luigjes and W. K. Kegel, *J. Phys. Chem. B*, 2011, **115**, 7175.
14 S. Hernandez-Navarro, J. Ignes-Mullol, F. Sagues and P. Tierno, *Langmuir*, 2012, **28**, 5981.
15 N. Kern and D. Frenkel, *J. Chem. Phys.*, 2003, **118**, 9882–9889.
16 J. Tavares, P. Teixeira and M. T. da Gama, *Mol. Phys.*, 2009, **107**, 453.
17 J. M. Tavares, P. I. C. Teixeira and M. M. Telo da Gama, *Phys. Rev. E*, 2009, **80**, 021506.
18 J. M. Tavares, P. I. C. Teixeira, M. M. T. da Gama and F. Sciortino, *J. Chem. Phys.*, 2010, **132**, 234502.
19 J. M. Tavares, P. I. C. Teixeira and M. M. Telo da Gama, *Mol. Phys.*, 2009, **107**, 453–466.
20 C. Gögelein, F. Romano, F. Sciortino and A. Giacometti, *J. Chem. Phys.*, 2012, **136**, 094512.
21 Z. Zhang, A. S. Keys, T. Chen and S. C. Glotzer, *Langmuir*, 2005, **21**, 11547.
22 I. C. Pons-Siepermann and S. C. Glotzer, *Soft Matter*, 2012, **8**, 6226.
23 M. Dijkstra, J. Hansen and P. A. Madden, *Phys. Rev. E*, 1997, **55**, 3044–3053.
24 E. Bianchi, G. Doppelbauer, L. Filion, M. Dijkstra and G. Kahl, *J. Chem. Phys.*, 2012, **136**, 214102.
25 E. Bianchi, R. Blaak and C. Likos, *Phys. Chem. Chem. Phys.*, 2011, **13**, 6297.
26 F. Sciortino and E. Zaccarelli, *Curr. Opin. Solid State Mater. Sci.*, 2011, **15**, 246.
27 A. Giacometti, F. Lado, J. Largo, G. Pastore and F. Sciortino, *J. Chem. Phys.*, 2009, **131**, 174114.
28 A. Giacometti, F. Lado, J. Largo, G. Pastore and F. Sciortino, *J. Chem. Phys.*, 2010, **132**, 174110.
29 F. Sciortino, A. Giacometti and G. Pastore, *Phys. Chem. Chem. Phys.*, 2010, **12**, 11869.
30 G. Munaó, D. Costa, F. Sciortino and C. Caccamo, *J. Chem. Phys.*, 2011, **134**, 194502.
31 G. Rosenthal, K. E. Gubbins and S. H. Klapp, *J. Chem. Phys.*, 2012, **136**, 174901.
32 A. Giacometti, *Cent. Eur. J. Phys.*, 2012, **10**, 540–551.
33 Z.-W. Li, Z.-Y. Lu, Z.-Y. Sun and L.-J. An, *Soft Matter*, 2012, **8**, 2693.
34 J. P. Hansen and I. R. McDonald, *Theory of Simple Liquids*, Academic Press, New York, 3rd edn, 2006.
35 C. Caccamo, *Phys. Rep.*, 1996, **274**, 1–105.
36 K.-H. Roh, D. C. Martin and J. Lahann, *Nat. Mater.*, 2005, **4**, 759–763.
37 B. Wang, B. Li, B. Zhao and C. Y. Li, *J. Am. Chem. Soc.*, 2008, **130**, 11594–11595.
38 C.-H. Chen, R. K. Shah, A. R. Abate and D. A. Weitz, *Langmuir*, 2009, **25**, 4320–4323.
39 A. M. Jackson, J. W. Myerson and F. Stellacci, *Nat. Mater.*, 2004, **3**, 330–336.
40 A. Walther and H. Müller, *Soft Matter*, 2008, **4**, 663.

41 Q. Chen, J. K. Whitmer, S. Jiang, S. C. Bae, E. Luijten and S. Granick, *Science*, 2011, **331**, 199.
42 B. S. Jiang, Q. Chen, M. Tripathy, E. Luijten, K. Schweizer and S. Granick, *Adv. Mater.*, 2010, **22**, 1060.
43 L. Hong, A. Cacciuto, E. Luijten and S. Granick, *Nano Lett.*, 2006, **6**, 2510–2514.
44 Q. Chen, J. Yan, J. Zhang, S. C. Bae and S. Granick, *Langmuir*, 2012, **28**, 13555.
45 J. Yan, M. Bloom, S. C. Bae, E. Luijten and S. Granick, *Nature*, 2012, **491**, 578.
46 H. Xie, Z.-G. She, S. Wang, G. Sharma and J. W. Smith, *Langmuir*, 2012, **28**, 4459.
47 G. Jackson, W. G. Chapman and K. Gubbins, *Mol. Phys.*, 1988, **65**, 1.
48 W. Bol, *Mol. Phys.*, 1982, **45**, 605.
49 L. W. Dahl and C. Andersen, *J. Chem. Phys.*, 1983, **78**, 1980.
50 W. R. Smith and I. Nezbeda, *J. Chem. Phys.*, 1984, **81**, 3694–3699.
51 J. Kolafa and I. Nezbeda, *Mol. Phys.*, 1987, **61**, 161–175.
52 I. Nezbeda, J. Kolafa and Y. V. Kalyuzhnyi, *Mol. Phys.*, 1989, **68**, 143–160.
53 F. Sciortino, A. Giacometti and G. Pastore, *Phys. Rev. Lett.*, 2009, **103**, 237801.
54 A. Reinhardt, A. J. Williamson, J. P. K. Doye, J. Carrete, L. M. Varela and A. A. Louis, *J. Chem. Phys.*, 2011, **134**, 104905.
55 B. D. Marshall, D. Ballal and W. G. Chapman, *J. Chem. Phys.*, 2012, **137**, 104909.
56 F. Romano and F. Sciortino, *Nat. Commun.*, 2012, **3**, 975.
57 C. Lara, I. Usov, J. Adamcik and R. Mezzenga, *Phys. Rev. Lett.*, 2011, **107**, 238101.
58 C. Lara, J. Adamcik, S. Jordens and R. Mezzenga, *Biomacromolecules*, 2011, **12**, 1868.
59 S. Raccosta, V. Martorana and M. Manno, *J. Phys. Chem. B*, 2012, **116**, 12078–12087.
60 A. G. Daful, J. B. Avalos and A. D. Mackie, *Langmuir*, 2012, **28**, 3730.